A&A 494, 287–294 (2009)
DOI: 10.1051/0004-6361:200810660

Astronomy & Astrophysics

Markov properties of solar granulation

A. Asensio Ramos

Instituto de Astrofísica de Canarias, 38205 La Laguna, Tenerife, Spain
e-mail: aasensio@iac.es

Received 23 July 2008 / Accepted 25 October 2008

ABSTRACT

Aims. We estimate the minimum length on which solar granulation can be considered to be a Markovian process.
Methods. We measure the variation in the bright difference between two pixels in images of the solar granulation for different distances between the pixels. This scale-dependent data is empirically analyzed to find the minimum scale on which the process can be considered Markovian.
Results. The results suggest that the solar granulation can be considered to be a Markovian process on scales longer than $r_{\mathrm{M}} = 300-500$ km. On longer length scales, solar images can be considered to be a Markovian stochastic process that consists of structures of size r_{M}. Smaller structures exhibit correlations on many scales simultaneously yet cannot be described by a hierarchical cascade in scales. An analysis of the longitudinal magnetic-flux density indicates that it cannot be a Markov process on any scale.
Conclusions. The results presented in this paper constitute a stringent test for the realism of numerical magneto-hydrodynamical simulations of solar magneto-convection. In future exhaustive analyse, the non-Markovian properties of the magnetic flux density on all analyzed scales might help us to understand the physical mechanism generating the field that we detect in the solar surface.

Key words. Sun: granulation – methods: statistical – Sun: atmosphere

1. Introduction

Advances in the study of stochastic processes (Van Kampen 1992) have led to the development of a powerful set of tools with which to infer important properties about complex physical systems. An example is the investigation of turbulence (Renner et al. 2001a), where the energy cascade from large to small scales is responsible for energy transfer in turbulent fluids (e.g. Frisch 1995). Another case of interest is the analysis of rough surfaces and interfaces (Jafari et al. 2003; Waechter et al. 2004), where the characterization of the roughness is of paramount importance for understanding the physical and chemical properties of these surfaces. Another example is the investigation of the complex time variation of the market (Renner et al. 2001b).

The characterization of such complex systems has been carried out historically based on notions of fractal theory. The idea is to verify the extent to which the cascade from larger to smaller scales follows a statistical self-similar behavior. In other words, given a physical quantity x that describes a property of the complex system (for instance, the velocity along a given axis of a fluid or the height for a surface), we investigate the fluctuation of this quantity on different scales. In general, it is assumed that the nth statistical moment of the fluctuation of x (also known as the structure function) fulfills:

$$\langle \Delta x(r)^n \rangle \propto r^{\xi_n}, \tag{1}$$

where r is the considered scale and ξ_n is an exponent that depends on n. If ξ_n depends linearly on n, it is said that the complex system is self-affine. In such a case, its properties are statistically invariant under a scale transformation, and the system is, consequently, self-similar or fractal. This was suggested by Kolmogorov (1941) for the turbulent cascade in fluid turbulence. If ξ_n is non-linear, the complex system is said to be multi-affine, and its properties must be defined using an infinity of scaling exponents. This is also true for more refined models of turbulence (Landau & Lifschitz 1987), in which the complex system exhibits what is referred to as multi-fractal properties. For more details about these models of turbulence, we refer to the book by Frisch (1995).

The problem with the scaling analysis is that complex systems exhibit scaling properties for a reduced range of scales. Following this procedure we then obtain only partial information about the statistical properties of the system. Furthermore, the range of scales under which the system presents scaling properties cannot be known a priori. For this reason, there has been increased interest in the statistical description of these complex systems by direct estimation of the probability distribution functions of the fluctuations on different scales, $p(\Delta x, r)$. Examples of this direct approach can be found in the literature (e.g. Friedrich et al. 2000; Ghasemi et al. 2006).

The crucial idea behind the new approach is the idea of identifying the complex system as a stochastic process in scales (differences of time and/or space) rather than purely in time or space. This different point of view allows us to obtain information about the correlation between different scales and analyze how the physical properties are related at different scales. Furthermore, it allows us to analyze the complex system without assuming regions of scaling behavior. As we show below, a substantial simplification in the statistical description of the system occurs if the Markovian property holds. In this case, the statistical properties on a given scale depend only on what happens on the next scale, and no correlation is found between other scales. Almost every stochastic process (at least many processes that are important in physics) can be considered Markovian on scales longer than a given threshold, which is usually referred to as the Markovian length r_{M} (or time, in case a process in time is being considered). The breaking of the Markovian property on scales below the threshold can be identified from the appearance

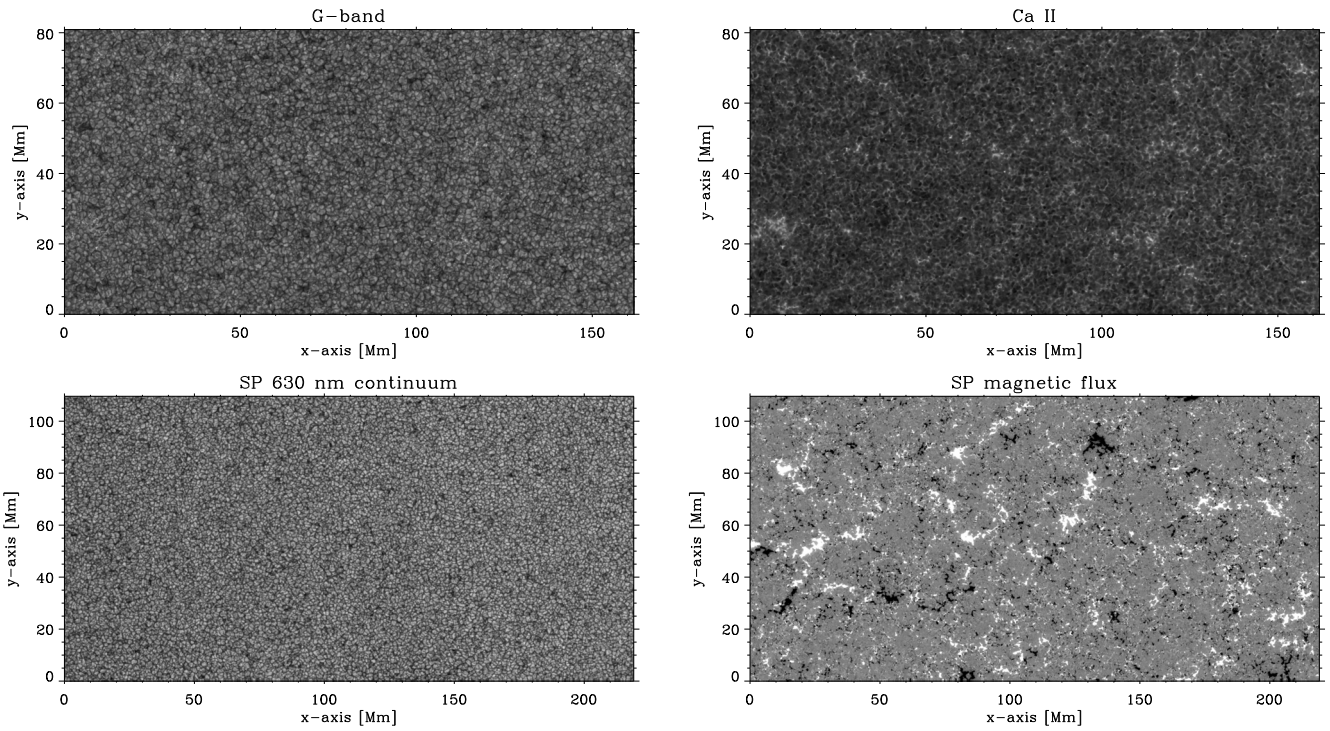

Fig. 1. Images used to analyze the Markovian properties of solar granulation. The images of *the upper pane* correspond to the G-band (*left*) and to Ca II H line, obtained with the broad-band filters. The images in *the lower panel* correspond to images obtained reconstructed from a scanning with the spectrograph, with the continuum intensity in *the left panel* and the magnetic flux density in *the right panel*.

of coherences in the system. For instance, the motion of a photon in a stellar atmosphere can be considered to be a Markovian process on scales above its mean free path.

Concerning solar research, Janßen et al. (2003) analyzed the fractal properties of observed images of small-scale magnetic structures in speckle-reconstructed magnetograms using the area-perimeter relation. They compared the results with magneto-convection simulations of the solar surface, and concluded that solar (and simulated) magnetograms are self-similar on a wide range of scales with a fractal dimension close to 1.4. Stenflo & Holzreuter (2002, 2003) demonstrated that the distribution of magnetic flux density appears to have fat tails (with respect to a Gaussian distribution) irrespective of the spatial resolution. They demonstrated this self-similarity by comparing full-disk magnetograms with both MDI magnetograms and data obtained at the Swedish La Palma Observatory. More recently, Abramenko (2005) considered the fact that magnetograms in active regions show several scaling regions and that the structure function must be considered multi-affine. A multi-fractal approach is then necessary and they found indications of time evolution in the multi-fractal properties of active regions, which can be associated with its degree of criticality.

We investigate the scales on which solar granulation can be considered to be a Markovian process in scale. This sheds some light on the scales involved in the generation of the granulation pattern. To this end, we investigate large images of solar granulation obtained with the *Hinode* satellite.

2. Observational material

The data that we analyze consists of two broad-band filter images taken with the Solar Optical Telescope (SOT, Tsuneta & et al. 2007) aboard *Hinode* on 2007 December 10 at 16:20. Additionally, we also analyzed the horizontal variation in the continuum intensity at 630 nm and the longitudinal magnetic flux density in an observation close to disk center carried out on 2007 March 10 starting at 11:37 and lasting for almost 3 h (Lites et al. 2008). The flux density was measured using the Stokes V profile observed with the SOT/SP in the Fe I doublet at 630 nm and using the weak-field approximation. We are aware that these measurements may differ from the true magnetic flux density because the fields may not be in the weak-field regime of the Zeeman effect. However, since we focus on the horizontal variation in the maps, small differences in the absolute value of the magnetic flux will not influence our conclusions significantly. The images are shown in Fig. 1. The image of the upper left panel is taken with a filter in the G-band and the image of the upper right panel is taken with a filter in the Ca II H line. The exposure time of these images is 0.1 s, and were centered on the disk center. After calculating the power spectrum of the image, we estimate the spatial resolution of the observations to be $\sim 0.24''$ (the scale on which the power spectrum is of the same level as the high frequency noise), a value that appears to be independent of the exact wavelength of the filter and is similar to the diffraction limit at 630 nm. The lower panel of Fig. 1 shows the continuum intensity (left) reconstructed from the slit scanning and the longitudinal magnetic flux density (right) images. The image in the G-band is representative of typical granulation with bright regions corresponding to magnetized regions. The image with the Ca II H filter presents a clear inverted granulation pattern with bright integranules and dark granules. Furthermore, bright regions can be seen coinciding with the bright points in the G-band image.

It is important to note that, instead of the magnetic flux density, one could have analyzed quantities such as B^2 that should be more related to the thermodynamical properties of the plasma. However, at the spatial resolution that can be achieved presently, the inference of the modulus of the magnetic field vector is, in

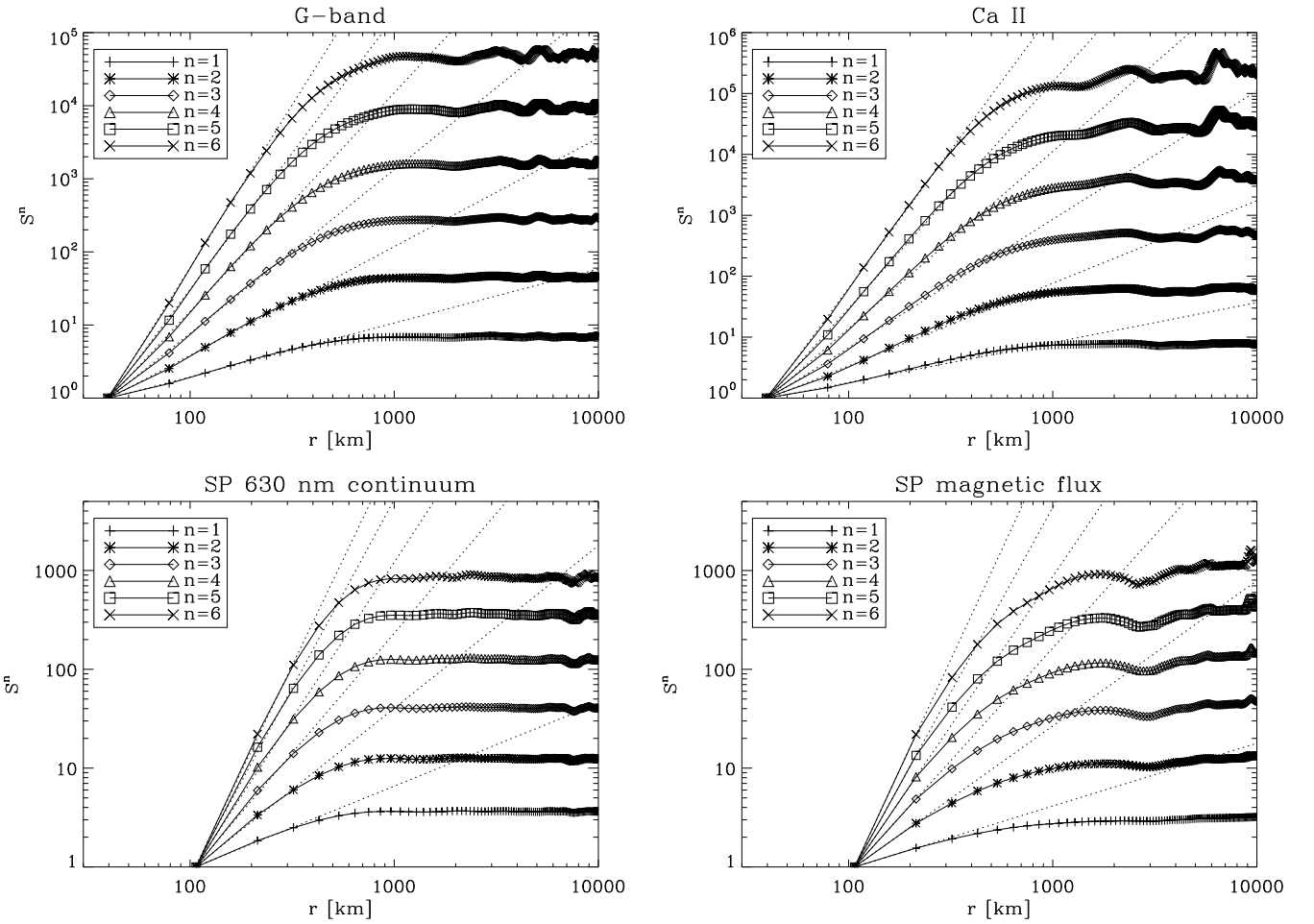

Fig. 2. Structure functions for the four considered images. The order corresponds to that found in Fig. 1. The length of the data allows to recover the structure function up to $n = 6$ without much noise. The dotted lines present linear fits to each S^n in the scaling region.

general, model-dependent. For this reason, we prefer to focus on the longitudinal magnetic flux density that is more straightforwardly related to the observables. We propose to analyze the markovian properties of other magnetic properties in future work.

We investigate the stochastic properties of the intensity increment:

$$h_r(x, y) = I(x', y') - I(x, y), \tag{2}$$

where $I(x, y)$ is the intensity of the image at pixel (x, y), while $I(x', y')$ is the value for a pixel located at a distance r (either in the horizontal or vertical direction). The intensity increment is a measure of the "roughness" of the image and describes the significance of the intensity variation on different scales. We extract series of 10^6 realizations of this quantity on each scale r for the broad-band images and 10^5 for the spectropolarimetric data by selecting points (x, y) in the field of view and verifying that the point (x', y') is inside the image. We consider various scales in the horizontal direction. However, we verified that no anisotropy is detected in the Markovian properties of the intensity increment when the same exercise is carried out in the vertical direction. One would expect some anisotropy in regions where the granulation is strongly modified by the presence of nearby structures, so that the physical processes responsible for the formation of the solar granulation can differ in different directions. For instance, the modified granulation pattern produced by the emergence of magnetic flux tubes simulated by Cheung et al. (2007) should produce anisotropies in the Markovian properties of the granulation pattern because of the privileged direction introduced by the presence of the flux tube.

3. Scaling analysis

Prior to empirically analyzing the statistical properties of the considered images, we investigate the scaling behavior of the structure functions:

$$S^n(r) = \langle h_r^n \rangle, \tag{3}$$

which are equivalent to the moments of the brightness fluctuation fields. First of all, it is important to note that the following analysis depends on the exact functional form of the fluctuation field, which we chose to be given by Eq. (2). The results are shown in Fig. 2, such that each panel is associated with the corresponding panels of Fig. 1. They indicate clearly that a scaling region ($S^n(r) \propto r^{\xi_n}$) is found in all cases on a subset of the considered values of r. If we choose the smallest scaling range, we find that the structure function for the G-band case is self-similar on scales below ∼200 km, while the value increases to ∼300 km for the Ca II H filter. Concerning the red continuum case, the scaling range is bounded from below around 100 km and from above at ∼300 km. Finally, the structure function for the magnetic flux can be considered self-similar only below ∼80 km. Note that the structure functions for the magnetic flux are far

noisier, probably due to the lower number of points in the image and significant amount of noise present because it is reconstructed from spectropolarimetric data.

The previous results indicate that all cases can be considered correctly to be self-affine because ξ_n depends linearly on n in the scaling range. Due to the relatively small size of the data series, the structure functions are only representative for $n \lesssim 6$. In this range, the following values are found for the slopes: $\xi_n(G-\text{band}) \propto 0.71n$, $\xi_n(\text{Ca II}) \propto 0.78n$, $\xi_n(\text{cont}) \propto 0.70n$, $\xi_n(\text{flux}) \propto 0.72n$.

4. Markov properties

4.1. Markov processes

We summarize the properties of Markov processes that we use in this paper. All these properties can be found in any suitable book on stochastic processes (e.g. Van Kampen 1992). We assume that the variable $h(r)$ defined by Eq. (2) fulfills a stochastic process in the scale r. To describe the stochastic process completely, we need to calculate the joint n-scale probability distribution function (PDF)[1] $p(h_1, r_1; h_2, r_2; \ldots; h_n, r_n)$, which indicates the probability of obtaining the value of the variable h_1 on scale r_1, the value h_2 on scale r_2, and, in general, the value h_n on scale r_n. We note that we assume that the scales are ordered following $r_1 < r_2 < \ldots < r_n$. Without losing generality, the joint PDF can be factorized by using the conditional PDFs, as

$$\begin{aligned} &p(h_1, r_1; h_2, r_2; \ldots; h_n, r_n) = \\ &p(h_1, r_1|h_2, r_2; \ldots; h_n, r_n) \cdot p(h_2, r_2|h_3, r_3; \ldots; h_n, r_n) \\ &\cdots\cdot p(h_{n-1}, r_{n-1}|h_n, r_n) p(h_n, r_n), \end{aligned} \tag{4}$$

where $p(h_n, r_n)$ is the probability of h_n being on scale r_n and $p(h_m, r_m|h_n, r_n)$ is the conditional probability, which indicates the probability of h_m being on scale r_m provided that h_n is found on scale r_n. The quantity $p(h_n, r_n)$ is known as the marginal probability distribution function, which is referred hereafter as PDF (on a given scale). According to Bayes' theorem, this conditional probability can be written as:

$$p(h_m, r_m|h_n, r_n) = \frac{p(h_m, r_m; h_n, r_n)}{p(h_n, r_n)} \,. \tag{5}$$

Although all the physics of the stochastic problem is contained in the joint PDF, unfortunately the joint PDF cannot be derived empirically, due to the enormous amount of data that one would require to complete such an estimation. Consequently, a simplification is mandatory, and can be created if one considers that the stochastic process can be classified as Markovian, so that:

$$p(h_1, r_1|h_2, r_2; \ldots; h_n, r_n) = p(h_1, r_1|h_2, r_2). \tag{6}$$

In other words, the probability of having h_1 on scale r_1, which in general depends on the complete history of the process on all scales, does only depend on the value of h_2 on scale r_2. Consequently, a Markov process is a process without memory, because the previous history of the process on different scales is of no relevance for calculating the probability of a future event. This simplifies Eq. (4) to read:

$$\begin{aligned} &p(h_1, r_1; h_2, r_2; \ldots; h_n, r_n) = p(h_1, r_1|h_2, r_2) \cdot p(h_2, r_2|h_3, r_3) \\ &\cdots\cdot p(h_{n-1}, r_{n-1}|h_n, r_n) p(h_n, r_n). \end{aligned} \tag{7}$$

[1] We use the term probability distribution function to refer to the probability density function, so that $p(x)$ provides the probability that a random variable assumes values between x and $x + \mathrm{d}x$. We note that, in the statistical literature, the probability distribution function usually refers to the cumulative distribution function $p(x \leq X)$.

The most straightforward consequence of the stochastic process being Markovian is that it can be fully described if one knows the conditional probability distribution function (CPDF) $p(h_{n-1}, r_{n-1}|h_n, r_n)$. The empirical determination of the CPDF is feasible with a relatively reduced amount of data and is the objective of this work.

As a consequence of the relation given by Eq. (6) any Markovian process fulfills the Chapman-Kolmogorov equation:

$$p(h_1, r_1|h_2, r_2) = \int \mathrm{d}h_3 p(h_1, r_1|h_3, r_3) p(h_3, r_3|h_2, r_2), \tag{8}$$

for any value of r_3 such that $r_1 < r_3 < r_2$. A usual interpretation of the previous equation is that the probability of having h_1 on scale r_1 provided that h_2 is found on scale r_2 can be obtained because of the infinite "paths" through states on an intermediate scale r_3. The Chapman-Kolmogorov equation is of fundamental importance because it can be formulated in differential form, which becomes the well-known Kramers-Moyal expansion (Van Kampen 1992):

$$\frac{\partial}{\partial r} p(h, r) = \sum_{k=1}^{\infty} \left(-\frac{\partial}{\partial h}\right)^k D^{(k)}(h, r)\, p(h, r), \tag{9}$$

where $D^{(k)}(h, r)$ are the Kramers-Moyal coefficients, whose knowledge is sufficient to describe the Markovian stochastic process completely. Another simplification arises when only $D^{(1)}(h, r)$ (drift) and $D^{(2)}(h, r)$ (diffusion) are of importance, and the remaining coefficients are very close to zero. According to Pawula's theorem (Pawula 1967), this occurs provided that $D^{(4)}(h, r) \sim 0$. In this case, we derive the well-known Fokker-Planck equation:

$$\frac{\partial}{\partial r} p(h, r) = -\frac{\partial}{\partial h} D^{(1)}(h, r)\, p(h, r) + \frac{\partial^2}{\partial h^2} D^{(2)}(h, r)\, p(h, r). \tag{10}$$

The coefficients $D^{(1)}(x, r)$ and $D^{(2)}(x, r)$ can be estimated empirically from a large set of data (Friedrich et al. 2000), which allows us to describe fully the statistical properties of the stochastic process by the solution of the Fokker-Planck equation, directly obtaining the PDF, $p(h, r)$ or the conditional PDFs, $p(h_1, r_1|h_2, r_2)$. The scope of this paper is to verify the Markovian properties of solar granulation. The possibility of using a Fokker-Planck equation to describe the granulation as a random field on scales will be assesed in a future paper. This would allow us, for instance, to construct artificially granulation images that have the same statistical properties as the real ones.

4.2. Empirical results

Figure 3 shows the PDF, $p(h, r)$, on different scales as indicated in the legend. Due to the difference in pixel size between the broad-band images and the spectropolarimetric data we note that the length scales at which the magnetic flux and the continuum at 630 nm are analyzed are a factor ~2.5 larger than for the broad-band images. The brightness difference h_r on all scales is normalized by the standard deviation of h_r on the largest scale, i.e., σ_∞, whose respective values are indicated in each panel of Fig. 3. The results for the G-band are distributions that are close to Gaussians except in the extreme tails. On scales larger than the largest shown in Fig. 3, the PDFs overlap. The bumps around $h_r/\sigma_\infty \approx 2.5$ and $h_r/\sigma_\infty \approx -2$ might be associated with the presence of bright points that induce larger fluctuations than one would expect without these bright points. This conclusion is reinforced by the fact that the results for the continuum at 630 nm

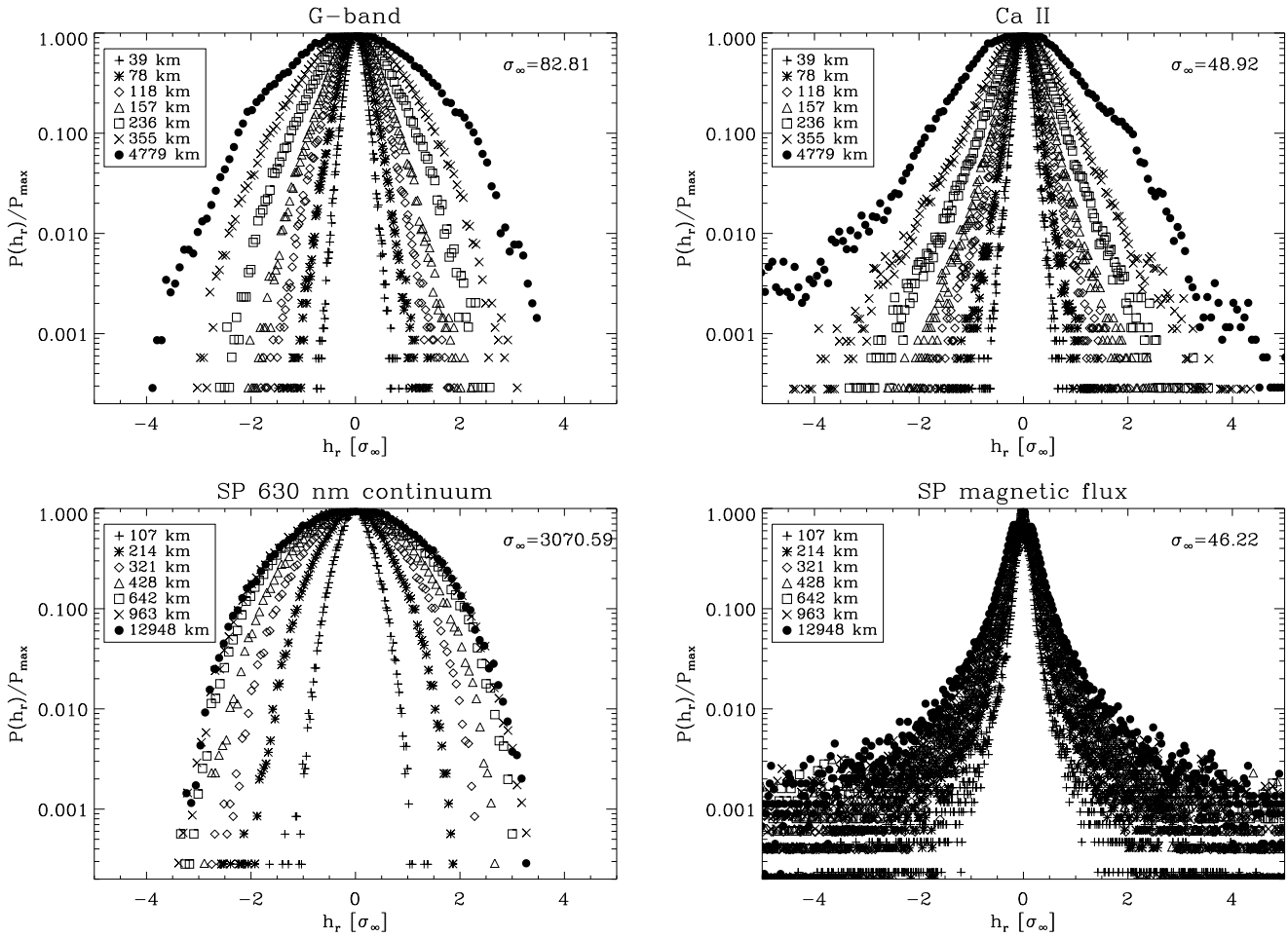

Fig. 3. Unconditional pdf $p(h, r)$ for a set of scales indicated in the legend. The values of h_r are normalized to σ_∞ calculated for the largest value of r whose value is indicated in each panel. The panels correspond to the G-band (*upper left panel*), Ca II H (*upper right panel*), continuum at 630 nm (*lower left panel*) and magnetic flux (*lower right panel*).

do not exhibit such bumps. For comparison, we emphasize that the PDF of fluctuations in pure Gaussian noise is normal with $\sigma = \sqrt{2}\sigma_\infty$, independent of scale. The results shown in Fig. 3 indicate that noise is not dominant because the PDFs vary with scale. Of interest is the fact that the PDFs for the Ca II H filter present heavy tails that cannot be explained by a Gaussian distribution. This is a consequence of the appearance of bright and dark points in the image (produced by the presence of strongly magnetized regions). Furthermore, large variations in the brightness difference can be found on almost all scales, producing fat tails of exponential type. A similar behavior is found in the flux distribution. In this case, however, the PDFs differ significantly from Gaussian with tails that have a Lorentzian shape. The fat tails found for the flux PDF are indicative of a strongly intermittent process, in which significant fluctuations have an unusually high probability of occurring compared to that for a Gaussian process. Similar PDFs but for the flux distribution itself were obtained by Stenflo & Holzreuter (2002, 2003), which apparently also exhibited a Lorentzian shape independent of scale.

Although the images are large, the use of Eq. (6) is insufficient for estimating the Markovian properties on all scales. However, it is sufficient for testing the Markovian character on three scales:

$$p(h_1, r_1|h_2, r_2) = p(h_1, r_1|h_2, r_2 = r1 + \Delta r; h_3 = 0, r_3 = r_1 + 2\Delta r), \quad (11)$$

where we chose $h_3 = 0$ and $r_2 - r_1 = r_3 - r_2 = \Delta r$ for simplicity. In any case, we verified that the same results were obtained for different values of h_3. The previous equality must be verified for all values of Δr and h_2. Figure 4 presents some examples of the conditional PDFs $p(h_1, r_1|h_2, r_2)$ and $p(h_1, r_1|h_2, r_2 = r1 + \Delta r; h_3 = 0, r_3 = r_1 + 2\Delta r)$, where the values of r_1 and Δr are given in the caption. The empirical conditional PDFs were calculated by constructing two-dimensional histograms. We present cuts along $h_2 = \pm\sigma_\infty$ below each contour plot. Although not exhaustive, the calculations demonstrate that the processes are not Markovian for the smallest value of Δr, while $p(h_1, r_1|h_2, r_2)$ and $p(h_1, r_1|h_2, r_2 = r1 + \Delta r; h_3 = 0, r_3 = r_1 + 2\Delta r)$ almost overlap for the largest value of Δr. This only happens for the G-band, Ca II H, and continuum images, and implies that there is a threshold scale smaller than which the stochastic process generating the images cannot be considered to be Markovian, while the process is Markovian above this scale. In contrast, the calculations for the magnetic flux indicate that, apparently, there is no scale above which the process can be considered to be Markovian.

Since a more thorough characterization of the Markovian properties is desired, we applied the Wilcoxon test (see, e.g. Renner et al. 2001a) that we briefly describe. We assume that x and y are two stochastic variables with unknown probability distribution functions $p(x)$ and $p'(y)$, respectively. By using the two samples $\{x_i, i = 1, \ldots, n\}$ and $\{y_j, j = 1, \ldots, m\}$, the Wilcoxon

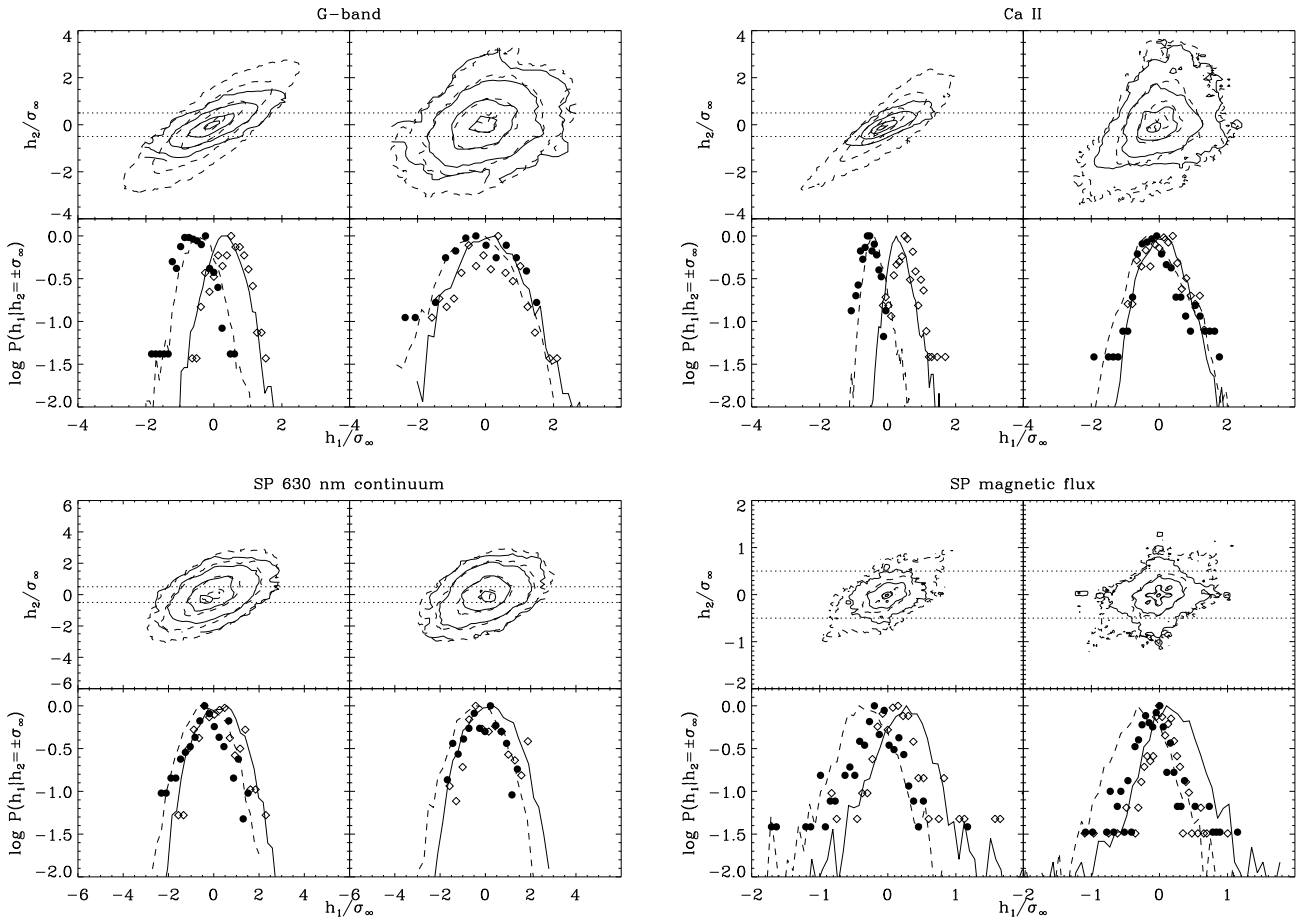

Fig. 4. Each block of four plots in this figure presents contour plots of the conditional pdfs $p(h_1, r_1|h_2, r_1 + \Delta r)$ (solid lines) and $p(h_1, r_1|h_2, r_1 + \Delta r; h_3 = 0, r_1 + 2\Delta r)$ (dashed lines) to verify the Markovian character of the brightness fluctuation, together with two cuts at $h_2 = \pm\sigma_\infty/2$. Each block of four plots corresponds to each image in Fig. 1. For the G-band and Ca II H data, we have used $r_1 = 395$ km while $\Delta r = 198$ km for the left panel of each block and $\Delta r = 1185$ km for *the right panel* of each block. For the spectropolarimetric data (continuum at 630 nm and magnetic flux), these values are $r_1 = 1070$ km and $\Delta r = 535$ km (*left panel*) and $\Delta r = 3210$ km (*right panel*).

test verifies whether the two PDFs $p(x)$ and $p'(y)$ are equivalent. In our case, since we wish to verify the validity of Eq. (11), x_i corresponds to samples of the brightness fluctuation h_1 on scale r_1 where h_2 has been found on scale r_2, while y_j corresponds to samples of h_1 on scale r_1 where h_2 and h_3 have been found on scales r_2 and r_3, respectively. The test sorts the realizations of x and y in ascending order and counts the number of inversions. In other words, for each value of y_j, we count the total number Q of values x_i that fulfill $x_i < y_j$. In the case that $p(x) = p'(y)$, the quantity Q is distributed normally about $\langle Q\rangle = mn/2$ with variance $\sigma_Q^2 = mn(m + n + 1)/12$. Consequently, the average value of the quantity $t = |Q - \langle Q\rangle|/\sigma_Q$ over h_2 fulfills $\langle t\rangle = \sqrt{2/\pi}$.

Applying the previous test to the brightness fluctuation fields, we obtained the results shown in Fig. 5. We first focus on our results for the G-band, Ca II H, and continuum. The value of $\langle t\rangle$ for many values of r_1 and Δr support the assertion that the process is Markovian above a scale that is in the range 300−500 km and the Markovian properties are maintained on larger scales. Above $\Delta r = r_M$ and apart from the dispersion produced by the presence of statistical noise in the determination of $\langle t\rangle$, all values are distributed about the value $\sqrt{2/\pi} \approx 0.8$, which implies that the two distributions of Eq. (11) can be assumed to be the identical. We verified that the same results for $\langle t\rangle$ are obtained when other values of h_3 are chosen, which demonstrates the reliability of the determination of the Markovian scale.

The previous analysis demonstrates that there are slight differences between the value of r_M for different images, with a larger value being measured for the Ca II H filter ($r_M \sim 500$ km) than for both the G-band and the continuum at 630 nm ($r_M \sim 300$ km). Therefore, the images can be considered as structures of sizes approximately equal to r_M that are described by a Markovian stochastic process. Above r_M, the brightness fluctuations on a given scale depend only on the next largest scale (as in a hierarchical cascade) and whatever the nature of the fluctuation is on a large scale, it does not affect directly the fluctuations on small scales. A direct consequence of the Markovian character is that the PDF can be described by the diffusion memoryless Fokker-Planck equation (provided that $D^{(4)}(h, r) \sim 0$) and can be considered to be a diffusion process on a range of different scales. Following previous works (e.g. Friedrich et al. 2000), the Fokker-Planck equation can be reconstructed empirically by estimating the drift and diffusion coefficients. The numerical solution of the Fokker-Planck equation should allow us to generate artificial images that have the same statistical properties as the observed ones, although this is presently ongoing work.

It is interesting to note that the derived r_M for the G-band and continuum cases is smaller than the average granular size,

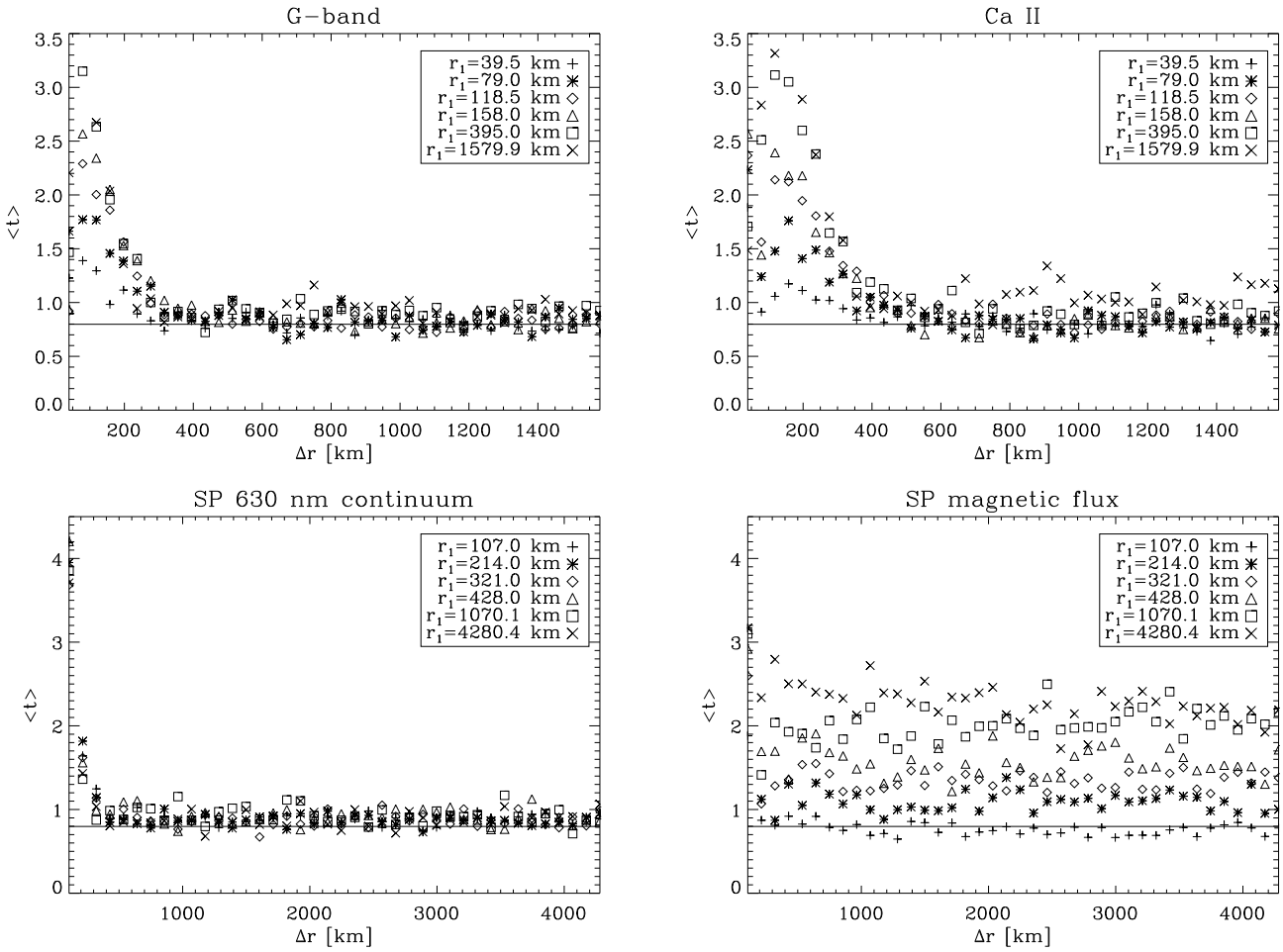

Fig. 5. Value of $\langle t \rangle$ for several values of r_1 and Δr The horizontal solid line indicates the value $\sqrt{2/\pi}$. Each panel corresponds to each panel of Fig. 1.

defined to be the FWHM of the autocorrelation function. The inner properties of structures with sizes smaller than r_M cannot be described by a Markov process because of the presence of coherences. As a consequence, their statistical properties cannot be described using either the Chapman-Kolmogorov or the Kramers-Moyal expansion, so that the structures must be characterized by determining the joint n-scale probability distribution function on all scales below r_M.

The results for the magnetic flux are remarkable because they imply that the stochastic process does not fulfill a Markovian process on any scale (except perhaps on the smallest considered scale when $r_1 = 107$ km). We verified that the same behavior for $\langle t \rangle$ was found when larger values of Δr (i.e. as large as several Mm) are considered. This behavior states that the probability distribution function of the magnetic flux fluctuations on a given scale depends on events occurring on all other scale. A more in-depth analysis of this fact could help us understand the relation between the lack of Markovian character and the physical mechanism generating the magnetic field (Asensio Ramos et al. 2009, in preparation).

5. Conclusions

We have presented an in-depth analysis of the stochastic properties of the difference in the brightness of two pixels separated by a distance r. The solar telescope onboard Hinode was used to obtain broad-band filter images. We estimated the limiting scale above which the stochastic process could be considered to be Markovian. Application of the Wilcoxon test implied that on scales above 300 km for the G-band and red continuum images, and above 500 km for Ca II H data, a Markovian behavior is exhibited. In such a case, the brightness fluctuation on a given scale depends only on events on the immediate larger scale. We also applied the same analysis to the magnetic flux inferred from spectropolarimetric observations carried out with SOT/SP onboard Hinode. The results indicated that the fluctuations in the magnetic flux cannot be considered to be Markovian, so that the PDF on a given scale depends on what is happening on all other scales.

The completely different behaviors of the brightness and magnetic flux imply that this should also be found for any successful numerical MHD simulation of solar magneto-convection (Vögler et al. 2005; Stein & Nordlund 2006). Since this test analyzes how the physical quantities change on different scales and how they are related, we can investigate if the sizes of the computational boxes are of the correct size for capturing the true behavior of the turbulent convection and the ensuing motion of the magnetic field. The present MHD simulations are carried out in quite small computational boxes (of the order of 6×6 Mm^2), and it remains to be determined the extent to which the analysis that we have presented here can be applied to far smaller fields-of-view.

Acknowledgements. I thank H. Frisch and J. Trujillo Bueno for useful comments on the manuscript. This research has been funded by the Spanish Ministerio de Educación y Ciencia through project AYA2007-63881.

References

Abramenko, V. I. 2005, Sol. Phys., 228, 29
Cheung, M. C. M., Schüssler, M., & Moreno-Insertis, F. 2007, A&A, 467, 703
Friedrich, R., J., P., & Renner, C. 2000, Phys. Rev. Lett., 84, 5224
Frisch, U. 1995, Turbulence (Cambridge University Press)
Ghasemi, F., Bahraminasab, A., Sadegh Movahed, M., et al. 2006, J. Stat. Mech., 11008
Jafari, G. R., Fazeli, S. M., Ghasemi, F., et al. 2003, Phys. Rev. Lett., 91, 226101
Janßen, K., Vögler, A., & Kneer, F. 2003, A&A, 409, 1127
Kolmogorov, A. N. 1941, Dokl. Akad. Nauk. SSSR, 30, 301
Lites, B. W., Kubo, M., Socas-Navarro, H., et al. 2008, ApJ, 672, 1237
Pawula, R. F. 1967, Phys. Rev., 162, 186
Renner, C., J., P., & Friedrich, R. 2001a, J. Fluid Mech., 433, 383
Renner, C., Peinke, J., & Friedrich, R. 2001b, Physica A, 298, 499
Stein, R. F., & Nordlund, Å. 2006, ApJ, 642, 1246
Stenflo, J. O., & Holzreuter, R. 2002, in SOLMAG 2002. Proceedings of the Magnetic Coupling of the Solar Atmosphere Euroconference, ed. H. Sawaya-Lacoste, ESA SP, 505, 101
Stenflo, J. O., & Holzreuter, R. 2003, in Current Theoretical Models and Future High Resolution Solar Observations: Preparing for ATST, ed. A. A. Pevtsov, & H. Uitenbroek, ASP Conf. Ser., 286, 169
Tsuneta, S., et al. 2007, Sol. Phys., submitted
Vögler, A., Shelyag, S., Schüssler, M., et al. 2005, A&A, 429, 335
Van Kampen, N. G. 1992, Stochastic Processes in Physics and Chemistry (North Holland)
Waechter, M. F. R., Schimmel, T., Wendt, U., & Peinke, J. 2004, Eur. J. Phys. B, 41, 259